Mid-Infrared nonlinear silicon photonics

Xiaoping Liu*[a], Bart Kuyken[b], William M. J. Green[c], Richard M. Osgood, Jr.[d], Roel Baets[c], Gunther Roelkens[c]

[a]Department of Optical Engineering and Quantum Electronics, Nanjing University, Nanjing, Jiangsu 210093, China; [b]Photonics Research Group, Department of Information Technology, Ghent University – imec, Ghent, Belgium; [c]IBM Thomas J. Watson Research Center, 1101 Kitchawan Road, Yorktown Heights, New York 10598, USA; [d]Department of Electrical Engineering, Columbia University, New York, New York 10027, USA

ABSTRACT

Recently there has been a growing interest in mid-infrared (mid-IR) photonic technology with a wavelength of operation approximately from 2-14 μm. Among several established mid-IR photonic platforms, silicon nanophotonic platform could potentially offer ultra-compact, and monolithically integrated mid-IR photonic devices and device arrays, which could have board impact in the mid-IR technology, such as molecular spectroscopy, and imaging. At room temperature, silicon has a bandgap ~ 1.12 eV resulting in vanishing two-photon absorption (TPA) for mid-IR wavelengths beyond 2.2 μm, which, coupled with silicon's large nonlinear index of refraction and its strong waveguide optical confinement, enables efficient nonlinear processes in the mid-IR. By taking advantage of these nonlinear processes and judicious dispersion engineering in silicon waveguides, we have recently demonstrated a handful of silicon mid-IR nonlinear components, including optical parametric amplifiers (OPA), broadband sources, and a wavelength translator. Silicon nanophotonic waveguide's anomalous dispersion design, providing four-wave-mixing (FWM) phase-matching, has enabled the first demonstration of silicon mid-IR optical parametric amplifier (OPA) with a net off-chip gain exceeding 13 dB. In addition, reduction of propagation losses and balanced second and fourth order waveguide dispersion design led to an OPA with an extremely broadband gain spectrum from 1.9-2.5 μm and >50 dB parametric gain, upon which several novel silicon mid-IR light sources were built, including a mid-IR optical parametric oscillator, and a supercontinuum source. Finally, a mid-IR wavelength translation device, capable of translating signals near 2.4 μm to the telecom-band near 1.6 μm with simultaneous 19 dB gain, was demonstrated.

Keywords: Silicon Photonics, nonlinear optics, mid-infrared, four-wave mixing, parametric process

1. INTRODUCTION

Although the research of silicon photonic platform has entered into the forth decade, the enthusiasm towards building CMOS compatible on-chip photonic components and systems has never been higher. The rapid development of this field over the past decades was largely driven by the need of low-cost, highly-compact and mass-production-ready photonic communication system because of the inherent CMOS compatibility for the silicon photonic platform and high refractive index contrast[1]. Lately, a lot of effort has been devoted to explore novel application areas using the silicon photonic components fabricated with the same CMOS process, including mid-infrared silicon photonics[2-9], silicon bio-photonics[10-13], and other applications[14-15].

Here we focus on our recent development of silicon mid-infrared photonics especially the nonlinear aspect of it. Crystal silicon has a central symmetric lattice structure. Therefore its lowest-order nonlinearity is third-order nonlinearity or Kerr effect. The magnitude of third-order optical nonlinear susceptibility of bulk silicon is about 100 times larger than that of silica[16]. In the meanwhile, because the typical effective mode area of a silicon photonic wire is three orders of magnitude less than that of an optical fiber (0.1 μm^2 vs. 100 μm^2), the effective nonlinear parameter for a silicon photonic wire is five orders of magnitude larger than that of an optical fiber (100 $W^{-1}m^{-1}$ vs. 1 $W^{-1}km^{-1}$)[17]. As a result, strong nonlinear interaction between an optical field and a silicon photonic wire can be observed in a Si photonic wire

*xpliu@nju.edu.cn

with a length scale of only a few millimeters compared with several hundred of meters in the case of an optical fiber. In recent years, various nonlinear effects associated with silicon's third-order nonlinear susceptibility have been studied[17-20]. It is shown that the nonlinear efficiency in the telecom band is largely suppressed by the optical limiting effect due to silicon's two-photon absorption (TPA) loss as well as TPA induced free-carrier absorption (FCA) loss[17-19]. Although the FCA loss can be drastically suppressed by reducing the free carrier lifetime by means of reverse biasing and ion implantation, the inherent TPA for silicon remains unchanged.

An effective way to bypass the strong TPA in silicon is to shift the wavelength of operation from telecom to mid-infrared. At room temperature, silicon has a bandgap ~ 1.12 eV which corresponds to a linear absorption cut-off wavelength of 1.1 μm. Therefore the cut-off wavelength for TPA in silicon is about 2.2 μm. The vanishing two-photon absorption (TPA) for mid-infrared wavelengths beyond 2.2 μm[16], which, coupled with silicon's large nonlinear index of refraction and its strong waveguide optical confinement, enables efficient nonlinear processes in the mid-infrared. By taking advantage of these nonlinear processes and judicious dispersion engineering in silicon photonic wires, we have recently demonstrated a handful of silicon mid-IR nonlinear components, including optical parametric amplifiers (OPA)[3], broadband sources[6], a wavelength translator[2] and an optical parametric oscillator[21]. Silicon nanophotonic waveguide's anomalous dispersion design enabled by varying the wire cross-section and/or changing the surrounding materials, providing four-wave-mixing (FWM) phase-matching, has led to the first demonstration of silicon mid-IR optical parametric amplifier (OPA) with a net off-chip gain exceeding 13 dB. In addition, by exploiting a new phase-matching scheme with a balanced second and fourth order waveguide dispersion, an OPA with an extremely broadband gain spectrum from 1.9-2.5 μm and >50 dB parametric gain was demonstrated, upon which several novel silicon mid-IR light sources were built, including a mid-IR optical parametric oscillator, and a supercontinuum source. Finally, a mid-IR wavelength translation device, capable of translating signals near 2.4 μm to the telecom-band near 1.6 μm with simultaneous 19 dB gain, was demonstrated.

2. FOUR-WAVE MIXING PHASE-MATCHING

Degenerate nonlinear four-wave-mixing process involves annihilation of two pump photons and creation of a signal and an idler photon. Such nonlinear process requires both energy conservation and momentum conservation described by the following two equations[17,22],

$$\omega_p - \omega_s = \omega_i - \omega_p = \Delta\omega \tag{1}$$

$$\Delta k = 2\gamma_p P_p - \Delta k_l = 2\gamma_p P_p - \left(2\beta_0^p - \beta_0^s - \beta_0^i\right) = 0 \tag{2}$$

where ω_p , ω_s , and ω_i are the angular frequency for pump, signal and idler photon, γ_p is the effective nonlinear parameter, P_p is the peak pump power, and β_0^p , β_0^s ,and β_0^i are the propagation constant for pump, signal, and idler photon. Using a Taylor series, the frequency dependent propagation constant near pump frequency can be represented as

$$\beta(\Delta\omega) = \beta_0^p + \sum_1^\infty \frac{1}{n!}\frac{d^n\beta}{d\omega^n}\bigg|_{\beta=\beta_0^p} (\Delta\omega)^n = \beta_0^p + \sum_1^\infty \frac{1}{n!}\beta_n^p (\Delta\omega)^n \tag{3}$$

where β_n^p is pump's n[th]-order dispersion coefficient, and $\Delta\omega$ is the frequency detuning from pump. Thus, the linear part of phase mismatch for a degenerate FWM process described by Eq. (1) can be fully characterized by using the even waveguide-dispersion term at the pump-wavelength/frequency:

$$\Delta k_l = 2\beta_0^p - \beta_0^s - \beta_0^i = -2\sum_1^\infty \frac{\beta_{2n}^p}{(2n)!}(\Delta\omega)^{2n} \tag{4}$$

where $\Delta\omega = \left|\omega_p - \omega_s\right| = \left|\omega_p - \omega_i\right|$ as shown in Eq. (1) is the frequency detuning between pump and signal/idler. In case of small, frequency detuning, *i.e.* when working in a region near the pump, the linear (*i.e.* non-power dependent) phase matching behavior for a degenerate FWM process can be approximated by using the waveguide dispersion up to the second order such that $\Delta k_l \approx -\beta_2^p (\Delta\omega)^2$; in this case anomalous dispersion with negative β_2 can lead to phase matching. Indeed parametric gain can be achieved in a spectral region near the pump by pumping silicon nanophotonic wire in the anomalous dispersion regime. However in certain cases when parametric processes involve signal and idler wavelengths far from the pump (*i.e.* conversion of mid-IR signals to the telecom band), it becomes necessary to take

higher-order dispersion terms into account. When dispersion up to the 4th order β_4 is retained, the equation governing the power-dependent phase matching condition becomes

$$\Delta k = 2\gamma_p P_p - \Delta k_l = 0 \Rightarrow 2\gamma_p P_p \approx -\beta_2 (\Delta\omega)^2 - \beta_4 (\Delta\omega)^4 / 12. \quad (5)$$

Figure 1(a)-(d) shows the graphic solutions to Eq. (5) corresponding to four different nontrivial combinations of β_2^p and β_4^p. Solutions exist when the frequency-detuning-dependent $\Delta k_l = -\beta_2 (\Delta\omega)^2 - \beta_4 (\Delta\omega)^4 / 12$ curve intersects the constant value of $\Delta k_l = 2\gamma_p P_p$. Consider now the four quadrants of dispersion space: First, I) As shown in Figure 1(a), when both β_2 and β_4 are positive, there is no solution to Eq. (5), which indicates no phase-matching point. II) However, there exists one phase-matching point as shown in Figure 1(b), when β_2 remains positive but β_4 becomes negative. This region of dispersion space has been used to achieve amplification in fiber optical parametric amplifiers, which are pumped in the normal dispersion regime, where the fiber exhibits negative fourth-order dispersion. III) In addition, in case of both β_2 and β_4 exhibiting negative values as shown in Figure 1(c), there is only one phase matching point. IV) Finally Figure 1(d) shows the most interesting case where β_2 is negative but β_4 is positive. In some cases, as is shown by the example of the red-dotted curve, there is no phase matching point. This is due to the fact that the negative contribution to the linear phase mismatch term from 4th-order dispersion $-\beta_4 (\Delta\omega)^4 / 12$ suppresses the positive contribution from 2nd-order dispersion $-\beta_2 (\Delta\omega)^2$ and prevents the overall linear phase mismatch from reaching a value of $2\gamma_p P_p$. However, if 4th-order dispersion is somewhat smaller, the two dispersion orders can balance each other in the vicinity of $\Delta k_l = 2\gamma_p P_p$, as shown in the dashed-blue curve. In this case, there is a broad frequency-detuning range (indicated by the dashed-blue arrow) where the linear phase mismatching lies within the phase detuning range ($\delta k = 2\gamma_p P_p \pm 2\pi / L$, where L is the length of the waveguide[22]) as indicated in shadow area. This condition can enable very broadband phase matching and therefore broadband parametric amplification/wavelength conversion. Finally, if the positive contribution from β_2 is even larger , the peak linear phase mismatch will reach its maximum well above $2\gamma_p P_p$, as shown in the solid-black curve, thus giving rise to a second phase-matching point, around which parametric gain becomes possible, albeit over a narrow, almost discrete band as is indicated by an arrow in Figure 1(d).

Figure 1. Graphic solutions for Eq. (5) four different nontrivial combinations of β_2 and β_4 : (a) $\beta_2 > 0 \,\&\, \beta_4 > 0$, (b) $\beta_2 > 0 \,\&\, \beta_4 < 0$, (c) $\beta_2 < 0 \,\&\, \beta_4 < 0$, (d) $\beta_2 < 0 \,\&\, \beta_4 > 0$. In (d), dotted-red, dashed-blue and solid-black curves show three representative cases under the condition of $\beta_2 < 0 \,\&\, \beta_4 > 0$; dashed-blue arrow indicates broadband phase matching; solid-black arrows indicate two phase matching bands; PMB: phase matching band. Shadowed areas in (a)-(d) indicate the phase detuning, within which efficient FWM can be achieved.

3. EXPERIMENT RESULTS

3.1 First demonstration of a mid-infrared silicon parametric amplifier

The essential dispersion and nonlinearity characteristics for a silicon nanophotonic photonic wire operating in the mid-IR were engineered through varying the nanoscale dimensions of the silicon core, the refractive index of the cladding, and the waveguide mode polarization. The resulting geometry ultimately selected for fabrication is shown in the SEM cross-section image in Figure 2(a). The silicon waveguide core has dimensions of 700 nm × 425 nm, and is designed to operate in the fundamental quasi-TM mode near a wavelength of 2200 nm, as illustrated by the overlaid mode field profile. The nanoscale-engineered optical structure is precisely controlled using a combination of silicon epitaxy, deep-UV lithography, reactive ion etching, and dielectric deposition, within an advanced CMOS fabrication facility.

Figure 2. Engineered silicon photonic wire characteristics. (a), SEM cross-section of the 700 nm × 425 nm silicon wire. The color-map illustrates the E_y component of the fundamental quasi-TM mode at λ = 2200 nm. (b), Simulated dispersion coefficient D (blue curve) and effective nonlinearity parameter γ (red curve).

The calculated dispersion coefficient D and effective nonlinearity parameter γ for this specific silicon photonic wire configuration are plotted in Figure 2(b). The dispersion is designed to be zero at a wavelength of λ = 2260 nm. The pump wavelength is chosen at λ = 2170 nm such that the photonic wire possesses anomalous dispersion conditions required for broadband phase matching [23]. Strong optical confinement of the quasi-TM mode to the ~ 0.3 um^2 silicon core results in a large effective nonlinearity of γ = 110 $(W \cdot m)^{-1}$ at λ = 2170 nm. The propagation losses of this photonic wire near λ = 2200 nm were determined to be approximately 4 dB/cm at 2030 nm, to 10 dB/cm at 2500 nm using the cutback method, and a coupling loss from lensed fiber into the silicon nanophotonic waveguide was estimated to be approximately 6.5 +/- 1 dB/facet.

The mid-IR nonlinear characteristics of a 4 mm-long silicon nanophotonic waveguide are studied using a pump-probe scheme by simultaneously injecting picosecond pump pulses (FWHM ~ 2 ps, repetition rate = 76 MHz) centered at λ = 2170 nm along with a cw tunable mid-IR laser signal, and observing the resulting FWM at the waveguide output. The peak coupled pump power at the waveguide input is P_p ~ 27.9 W, while the input signal power P_{sig} is kept below 0.45 mW. For each spectrum shown Figure 3(a), two photons from the high-intensity pulsed pump mix with a single photon from the tunable *cw* signal to generate a wavelength-converted idler photon, at a wavelength dictated by energy conservation. The FWM process also produces an additional photon at the signal wavelength, which can ultimately contribute to signal amplification. Due to the pulsed nature of the pump, the generated idler and amplified signal also occurs as short pulses.

Figure 3. Mid-infrared FWM experiments and broadband on-chip optical parametric amplification**.** (a), Series of FWM spectra taken at the output of the 4-mm-long waveguide. (b), On-chip parametric signal gain (black triangles) and idler conversion gain (red circles), with bandwidth of ~ 220 nm and peak values > 25 dB. Net off-chip gain results where amplification exceeds fiber-chip insertion losses (blue line), with a maximum value of ~ 13 dB.

The experimental data reveals that the engineered silicon nanophotonic waveguide successfully functions as a mid-IR optical parametric amplifier (OPA), with very large maximum signal and idler gain values of 24 dB and 25.4 dB, respectively. Moreover, the on-chip parametric gain is significant enough to overcome substantial fiber-chip coupling losses (blue curve), demonstrating net off-chip gain as large as 10 dB for the signal and 13 dB for the idler. The overall on-chip gain bandwidth spans the range from 2060 nm to 2280 nm. The maximum parametric gain obtained using our ultra-compact 4 mm device is more than 100 times larger than previously observed in a 17 mm-long silicon waveguide pumped near λ = 1550 nm, where gain has been limited to ~3 dB owing to strong TPA-induced saturation effects. By operating the pump at longer wavelengths in the mid-IR, we have realized a chip-scale silicon nanophotonic OPA which breaks the limits set by TPA nonlinear absorption.

3.2 Ultra-broadband silicon parametric amplifier

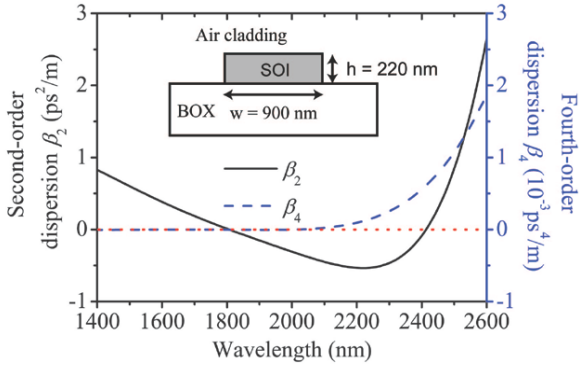

Figure 4. 2nd-order (solid black curve) and 4th-order (dashed blue curve) dispersion of fundamental quasi-TE mode for the silicon wire: w = 900 nm, h = 220 nm, as shown in inset.

As shown in Section 2, there exists an ultra-broadband phase-matching region when β_2 is negative but β_4 is positive at the pump wavelength. Such unique dispersion characteristics was obtained on a silicon photonic wire fabricated on a 200 mm silicon-on-insulator (SOI) wafer in a CMOS pilot line at *Ghent University-IMEC*. It had cross-sectional dimensions of w = 900 nm by h = 220 nm (inset Figure 4), and was 2 cm in length. The cladding consisted of air above and a 2 μm buried oxide (BOX) below the waveguide. The waveguide was designed to operate in the fundamental quasi-TE mode and had low propagation losses < 2.8 dB/cm for wavelengths from 2000 nm to 2500 nm. The waveguide loss here was reduced by more than 2× compared with that from prior work described in Section 3.1.

The simulated silicon photonic wire dispersion show that the engineered-waveguide dimensions produce anomalous dispersion conditions ($\beta_2 < 0$) at wavelengths between the two zero-dispersion wavelengths of 1810 nm and 2410 nm as shown Figure 4. Furthermore, this photonic wire has small positive 4th-order dispersion ($\beta_4 > 0$) within the same wavelength range due to the positive curvature of the 2nd-order dispersion graph. Therefore, the balanced opposing signs of β_2 and β_4 should permit broad and discrete phase matching when this silicon nanophotonic wire is pumped within the range 1810 nm - 2410 nm.

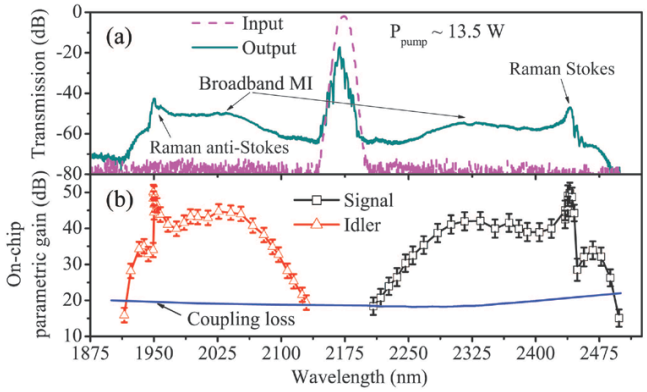

Figure 5. (a) Input (dashed magenta curve) and transmitted (solid cyan curve) pump spectra, illustrating broadband MI and Raman Stokes/anti-Stokes peaks. (b) On-chip parametric gain, exhibiting broadband on-chip amplification over a bandwidth > 580 nm, maximum Raman-assisted gain values of ~ 50 dB, unassisted FWM parametric gain of ~ 40 dB, and peak net off-chip gain > 30 dB.

A similar experiment setup and measurement technique to that used in the study discussed in Section 3.1 is employed to characterize the performance of parametric process. The input pump pulse has a center wavelength ~ 2175 nm and it shows a clean spectrum with a signal-to-noise ratio > 75 dB as illustrated by the dashed magenta curve in Figure 5(a). The peak pump power coupled into the silicon nanophotonic wire input is P_p ~ 13.5 W. Besides the usual self-phase modulation (SPM) represented by the oscillations on the central peak, and spectral blue-shift due to residual free-carrier dispersion (seen in comparison to the dashed magenta curve), the spectrum of transmitted pump (solid cyan curve of Figure 5(a)) exhibits significant modification compared with the input spectrum. The spectrum at the waveguide output is characterized by the emergence of a strong broadband MI spectrum extending from 1911 nm to 2486 nm. In addition, a prominent Raman Stokes peak rides on top of the MI spectrum at a wavelength of 2411 nm, frequency down-shifted from the pump by a Stokes shift of ~ 15.6 THz. Moreover, a frequency up-shifted Raman anti-Stokes peak at a wavelength of 1950 nm is visible. Furthermore, the small interference pattern visible around both narrowband Raman peaks originates from the additional phase shift introduced by the dispersion of the Raman susceptibility. This phase shift is superimposed upon the broadband FWM phase matching condition, producing spectral fringes where phase matching for MI is disrupted.

The strong MI background suggests that the on-chip mid-IR parametric gain available is far larger than previously discussed in Section 3.1; note that in these studies MI was hardly observed. To probe the gain a wavelength-varying *cw* signal is used. The *cw* signal power coupled into the waveguide is varied such that it is low enough to prevent gain saturation due to pump depletion but high enough to achieve a good visibility of the idler on top of the MI spectrum. The peak pump power remains the same as in the pump transmission measurement, P_p ~ 13.5 W. Figure 5(b) plots the measured on-chip amplification/conversion gain. The mid-IR-pumped silicon photonic wire OPA exhibits on-chip optical parametric amplification over a bandwidth exceeding 580 nm. Near the Raman peaks, the OPA reaches a maximum Raman-assisted parametric signal/idler gain of ~ 50 dB. The gain profile exhibits the residue of an interference pattern at a wavelength ~ 2445 nm on the signal side and ~ 1950 nm on the idler side around the Raman-assisted peaks related to that seen in the MI spectrum of Figure 5(a). The OPA shows a net off-chip gain bandwidth of ~ 550 nm, with ~ 30 dB Raman-assisted off-chip gain for both signal and idler after compensating for all fiber-chip coupling losses from both facets (~ 20 dB, solid blue curve in Figure 5(b)). However, the OPA can be shown to have a maximum net off-chip optical gain of larger than 20 dB resulting solely from the parametric FWM process. In addition in comparison with the earlier results reported in Section 3.1, the peak operating pump power is reduced to less than half.

At the same time, the maximum on-chip gain obtained using the 2 cm-long wire here shows an improvement of more than 25 dB, while the on-chip gain bandwidth is increased by more than 2.5×.

3.3 Supercontinuum generation from mid-infrared to telecom band in a silicon photonic wire

Using the same silicon photonic wire but shifting the pump wavelength to a value different from that used in the previous study in Section 3.2, a different phase-matching region could be obtain as discussed in Section 3.1. Figure 6 illustrates the evolution of the photonic wire's output spectrum as the input coupled peak pump power is gradually increased from 3.1 W (green trace) to 12.7 W (black trace). These spectra reveal that a number of different nonlinear processes ultimately combine to produce the broadband supercontinuum. At an input power of 3.1 W, the pump pulse train's spectrum is broadened significantly by self phase modulation (SPM), as illustrated by the numerous interference fringes appearing near 2120 nm. A series of sidebands are generated in the vicinity of the pump at 2120 nm. Closest to the pump, two broad sidebands (labeled as MI(1)) are generated near wavelengths of 1990 nm and 2250 nm. Further away from the pump, a pair of narrowband peaks (labeled as MI(2)) appear at wavelengths of 1870 nm and approximately 2510 nm. Both the broad and narrow sideband pairs originate from modulation instability, *i.e.* the amplification of background noise at wavelengths for which the phase matching condition in Eq. (5) above is satisfied. When the coupled peak pump power is increased to 4.3 W, the spectral intensity of the generated sidebands is observed to increase with respect to the pump, and the degree of pump and sideband broadening increases.

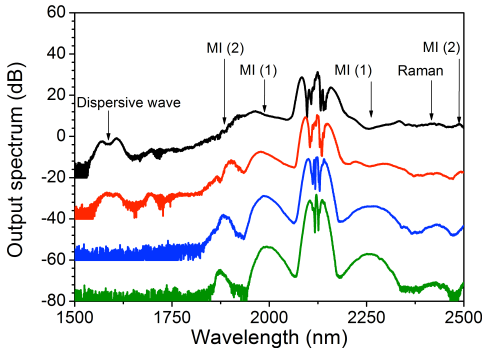

Figure 6. Measured output spectrum for increasing values of coupled input peak power: 3.1 W (green), 4.3 W (blue), 7.9 W (red) and 12.7 W (black). The spectra are vertically offset by multiples of 20 dB for clarity.

At a pump power of 7.9 W, several new spectral components are observed, peaked near 1700 nm and 1600 nm respectively. The term at 1700 nm is generated through cascaded four-wave mixing (FWM), where the original MI(2) peak at 1890 nm serves as the degenerate pump and the input pulse at 2120 nm acts as the signal. The peak around 1600 nm is believed to be the result of Cherenkov radiation referred to as dispersive wave generation[23]. At first sight this is unexpected when we compare the different length scales in our experiment. The nonlinear length is approximately L_{nl} = 500 μm at a coupled peak power of 12.7 W, whereas the soliton fission length is 6.3 cm, significantly longer than the wire waveguide's length. Therefore, generation of a dispersive wave through soliton fission is unlikely. However, recent research has shown that in the "long pulse" regime where modulation instability is the main driving force behind supercontinuum generation, dispersive waves can also be generated through the simultaneous formation of pre-solitonic breathers along the pump pulse[24,25].

There are several facts supporting this finding. First, the 1600 nm peak lies within the normal dispersion regime of the silicon wire, as expected for the generation of dispersive waves. In addition, there is no combination of the observed modulation instability and/or Raman peaks that can generate the 1600 nm component through cascaded FWM. Moreover, seeding the supercontinuum using a CW laser at 1600 nm does not reveal any parametric gain at this wavelength. This lack of gain excludes the possibility that the 1600 nm component is generated through the process of modulation instability phase-matched through even higher-order dispersion terms (e.g. β_6, β_8), which become important at large detuning from the pump.

Finally, at the highest pump power of 12.7 W, Figure 6 shows that the spectral broadening of all generated peaks leads to the merging of the MI(1), MI(2), and Raman peaks, and to increased flatness of the output spectrum on both the red and blue sides of the pump. Under these conditions, the supercontinuum output from the mid-IR pumped SOI wire waveguide extends from 1540 nm to beyond 2500 nm, the maximum wavelength resolved by the OSA used.

3.4 Discrete FWM as a wavelength translator

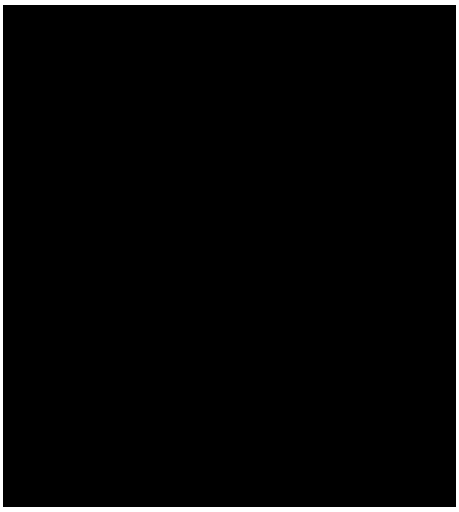

Figure 7. (a) Signal off: Modulation instability output spectrum generated by the exponential amplification of noise in the sidebands when pumping at 1946 nm. (b) Signal on: Parametric amplification of a continuous wave mid-IR signal at 2440 nm, and simultaneous conversion to a wavelength of 1620 nm.

As shown in the previous section, there exists a second MI peak which locates far from the pump spectrally in the experiment, which can be explained by the unique phase-matching condition as described in the Section 2. By selecting an appropriate pump wavelength, such spectral separation can be further enlarged to enable a wavelength translation process between mid-infrared and telecom band. Figure 7(a) and (b) show representative output spectra obtained with the pump pulse train (FWHM ~ 2 ps, repetition rate = 76 MHz) located at a wavelength of 1946 nm, with a peak power of 37.3 W coupled into the same silicon photonic wire described in the previous sections. In Figure 7(a) only the pump propagates through the silicon wire. The strong broadband MI near the pump and Raman Stokes are clearly seen. Moreover, two additional discrete bands originating from higher-order phase matching are also visible in the MI spectrum, located at λ = 1620 nm and at λ = 2440 nm. The output power in the 2440 nm peak is reduced due to higher input/output waveguide coupling losses at longer wavelengths. Figure 7(b) shows the spectrum when the discrete bands are probed by a *cw* mid-IR laser at 2440 nm. When the signal is tuned into this spectral band, it experiences exponential parametric gain, and is simultaneously wavelength converted to a telecom-band idler at 1620 nm. In addition, the signal and converted idler are broadened by cross-phase modulation due to the pulsed nature of the source.

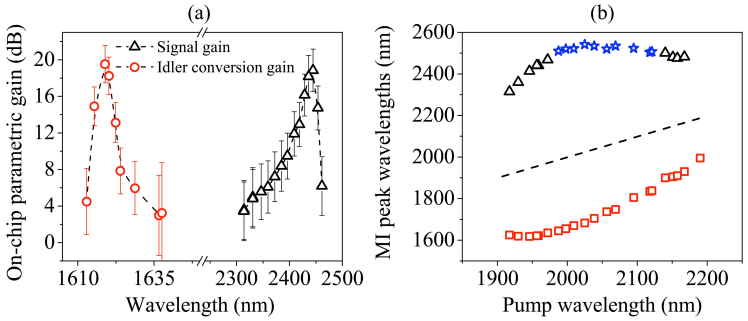

Figure 8. (a) On-chip parametric signal gain and idler-frequency conversion gain for the mid-infrared signals. Dashed lines are spline curves included to guide the eye. (b) Peak of the discrete modulation instability bands as a function of pump wavelength. The MI peaks indicated by the blue stars was not directly measurable, as they were located beyond the 2500 nm maximum-wavelength limit of the OSA used. Rather, the positions of these peaks were inferred from energy conservation. The dashed line tracks the position of the pump.

By recording a series of similar spectra at different signal wavelengths, the parametric amplification and conversion efficiency can be determined as a function of wavelength within the discrete phase-matching bands. This data is illustrated in Figure 8(a), indicating a peak net on-chip signal amplification of 18.8 dB and a conversion efficiency of

19.5 dB. The on-chip gain exceeds 10 dB over a bandwidth of 10 nm near the idler (1620 nm), and a bandwidth of 62 nm near the signal (2440 nm). The large values of idler-conversion gain indicate that silicon nanophotonic wires can potentially allow for efficient amplification of weak mid-IR signals and subsequent detection using commercially available high-sensitivity telecom receivers.

Figure 8(b) shows the location of the discrete bands as a function of pump wavelength (defined as the modulation-instability peak wavelength). Tuning the pump wavelength varies the dispersion at the pump and thus the linear phase mismatch accumulated along the silicon nanophotonic wire between pump, signal and idler waves (see Eq. 4), and results in a spectral shift of the discrete bands where phase matching is obtained. The spectral separation of the bands becomes larger with increasing $|\beta_2|$ and decreasing $|\beta_4|$. The data illustrates that the discrete bands move closer to the pump wavelength when the pump approaches the zero dispersion wavelengths at 1810 nm and 2410 nm, *i.e.* when the magnitude of β_2 decreases. Further optimization of the wire dimensions so as to increase the second-order dispersion while simultaneously decreasing the fourth-order dispersion would make it possible to design a silicon wire capable of converting mid-IR signals directly to the C-band near 1550 nm.

4. CONCLUSION

In this manuscript we show that by shifting the wavelength of operation from telecom band to mid-infrared parametric nonlinear process with very high efficiency can be achieved in silicon photonic wires as a result of vanishing TPA of silicon. In such scheme, we demonstrate the first parametric amplifier with net off-chip gain more than 10 dB in the mid-infrared region. By careful dispersion engineering, a major increase in the gain and bandwidth can be achieved for silicon photonic wire optical parametric amplifiers. In addition, we show that under certain phase-matching conditions enabled by selecting appropriate pump wavelength, supercontinuum generation from mid-infrared to telecom band is possible. Moreover, our work demonstrates use of higher-order phase matching in silicon photonic wires to realize the conversion of signals from the mid-IR into the telecommunication band with a signal amplification of 18.8 dB and a conversion gain of 19.5 dB. These results are important since they can be applied to the processing of weak mid-IR signals using established high-sensitivity telecom-band optical-receiver technology. Our results also potentially offer a large sensitivity enhancement over traditional direct mid-IR detection approaches using narrow band-gap semiconductors. Finally, our work shows that judicious dispersion engineering and improved wire loss characteristics can be leveraged to control and improve the bandwidth and gain, perhaps even extending the broad/discrete gain band to telecom wavelengths *even near 1550 nm*.

REFERENCES

[1] Reed, G. T., [Silicon Photonics: The State of the Art], John Wiley & Sons, New York, NY, USA, 2008.

[2] Liu X. P., Kuyken B., Roelkens G., Baets R., Osgood R. M., and Green W. M. J., "Bridging the mid-infrared-to-telecom gap with silicon nanophotonic spectral translation", Nature Photonics 6, 667-671 (2012).

[3] Liu X. P., Osgood R. M., Vlasov Y. A., and Green W. M. J., "Mid-infrared optical parametric amplifier using silicon nanophotonic waveguides," Nature Photonics 4, 557 - 560 (2010).

[4] Liu X. P., Driscoll J. B., Dadap J. I., Osgood R. M., Assefa S., Vlasov Y. A., and Green W. M. J., " Self-phase modulation and nonlinear loss in silicon nanophotonic wires near the mid-infrared two-photon absorption edge," Optics Express 19, 7778-7789 (2011).

[5] Kuyken B., Liu X. P., Roelkens G., Baets R., Vlasov Y. A., Osgood R. M., and Green W. M., "50 dB parametric on-chip gain in silicon photonics wires," Optics Letters 36, 4401-4403 (2011)

[6] Kuyken B., Liu X. P., Osgood R. M., Vlasov Y. A., Baets R., Roelkens G., and Green W. M., "Mid-infrared to telecom-band supercontinuum generation in highly nonlinear silicon-on-insulator wire waveguides," Optics Express 19, 20172-20181 (2011).

[7] Shankar R., Leijssen R., Bulu I., and Lončar M., "Mid-infrared photonic crystal cavities in silicon," Optics Express 19, 5579-5586 (2011).

[8] Milošević M. M., Nedeljkovic M., Ben Masaud T. M., Jaberansary E., Chong H. M. H., Emerson N. G., Reed G. T. and Mashanovich G. Z., "Silicon waveguides and devices for the mid-infrared", Appl. Phys. Lett. 101, 121105 (2012).

[9] Soref R., "Mid-infrared photonics in silicon and germanium", Nature Photonics 4, 495 - 497 (2010).

[10] Wang X., Flueckiger J., Schmidt S., Grist S., Fard S. T., Kirk J., Doerfler M., Cheung K. C., Ratner D. M., and Chrostowski L., "A silicon photonic biosensor using phase-shifted Bragg gratings in slot waveguide", Journal of Biophotonics 6, 821–828 (2013).
[11] Goykhman I., Desiatov B. and Levy U., "Ultrathin silicon nitride microring resonator for biophotonic applications at 970 nm wavelength", Appl. Phys. Lett. 97, 081108 (2010).
[12] Iqbal, M., Gleeson, M.A., Spaugh, B., Tybor, F., Gunn, W.G., Hochberg, M., Baehr-Jones, T., Bailey, R.C., and Gunn, L.C., "Label-Free Biosensor Arrays Based on Silicon Ring Resonators and High-Speed Optical Scanning Instrumentation", IEEE Journal of Selected Topics in Quantum Electronics 16, 654 – 661 (2010).
[13] Xu D.-X., Vachon M., Densmore A., Ma R., Delâge A., Janz S., Lapointe J., Li Y., Lopinski G., Zhang D., Liu Q. Y., Cheben P., and Schmid J. H., "Label-free biosensor array based on silicon-on-insulator ring resonators addressed using a WDM approach", Optics Letters 35, 2771-2773 (2010).
[14] Van Acoleyen K., Rogier H., and Baets R., "Two-dimensional optical phased array antenna on silicon-on-insulator", Optics Express 18, 13655-13660 (2010).
[15] Sun J., Timurdogan E., Yaacobi A., Shah Hosseini E., and Watts M. R., "Large-scale nanophotonic phased array", Nature 493, 195–199 (2013).
[16] Bristow A. D., Rotenberg N., and van Driel H. M., "Two-photon absorption and Kerr coefficients of silicon for 850-2200 nm," Applied Physics Letters 90, 191104-191106 (2007).
[17] Osgood R. M., Panoiu N. C., Dadap J. I., Liu X., Chen X., Hsieh I. W., Dulkeith E., Green W. M. J., and Vlasov Y. A., "Engineering nonlinearities in nanoscale optical systems: physics and applications in dispersion-engineered silicon nanophotonic wires," Advances in Optics and Photonics 1, 162-235 (2009).
[18] Leuthold J., Koos C. and Freude W., "Nonlinear silicon photonics", Nature Photonics 4, 535 - 544 (2010).
[19] Foster M. A., Turner A. C., Lipson M., and Gaeta A. L., "Nonlinear optics in photonic nanowires", Optics Express 16, 1535-1547 (2008).
[20] Lin Q., Painter O. J., and Agrawal G. P., "Nonlinear optical phenomena in silicon waveguides: Modeling and applications", Optics Express 15, 16604-16644 (2007).
[21] Kuyken B., Liu X., Osgood, Jr. R. M., Baets R., Roelkens G., and Green W. M. J., "A silicon-based widely tunable short-wave infrared optical parametric oscillator", Optics Express 21, 5931-5940 (2013).
[22] Agrawal G. P., [Nonlinear Fiber Optics], Academic, San Diego, (2001).
[23] Akhmediev N. and Karlsson M., "Cherenkov radiation emitted by solitons in optical fibers", Phys. Rev. A 51, 2602 (1995).
[24] Mussot A., Lantz E., Maillotte H., Sylvestre T., Finot C., and Pitois S., "Spectral broadening of a partially coherent CW laser beam in single-mode optical fibers", Opt. Express 12, 2838-2843 (2004).
[25] Dudley J. M., Genty G., Dias F., Kibler B., and Akhmediev N., "Modulation instability, Akhmediev Breathers and continuous wave supercontinuum generation", Opt. Express 17, 21497-21508 (2009).